An expanding thermal plasma for deposition of a-Si:H

AN EXPANDING THERMAL PLASMA FOR DEPOSITION OF a-Si:H

R.J. SEVERENS, G.J.H. BRUSSAARD, H.J.M. VERHOEVEN, M.C.M. VAN DE SANDEN AND D.C. SCHRAM
Department of Physics, Eindhoven University of Technology, P.O. Box 513, 5600 MB Eindhoven, Netherlands

ABSTRACT

A remote argon/hydrogen plasma is used to deposit amorphous hydrogenated silicon. The plasma is generated in a DC thermal arc (typical operating conditions 0.5 bar, 5 kW) and expands into a low pressure chamber (20 Pa) thus creating a plasma jet with a typical flow velocity of 10^3 m/s. Pure silane is injected into the jet immediately after the nozzle, in a typical flow mixture of $Ar:H_2:SiH_4$=55:10:6 scc/s. The electron temperature in the jet is low (typ. 0.3 eV): silane radicals are thought to be produced mainly by hydrogen abstraction, but also by a sequence of dissociative charge exchange and consecutive dissociative recombination.

In-situ ellipsometry yields refractive indices of 3.6-4.2 at 632.8 nm and growth rates of 10-20 nm/s. FTIR analysis yields a hydrogen content of 9-25 at.% and refractive indices of 2.7-3.3 in the infrared. The SiH density decreases with increasing hydrogen content, whereas the SiH_2 density increases. Above 11 at.%, the majority of hydrogen is bonded in the SiH_2 configuration. The optical bandgap remains constant at approximately 1.72 eV. The photoconductivity is of the order 10^{-6} $(\Omega cm)^{-1}$ and the photoresponse 10^6.

INTRODUCTION

In cost reduction of amorphous silicon based large area applications such as photovoltaic cells, upscaling is a major issue. A new approach gaining much attention is roll-to-roll deposition on flexible substrates [1], where a high deposition rate is desired. Furthermore, Ganguly and Matsuda have argued that at elevated substrate temperatures (>350 °C), the defect density decreases with increasing deposition rate [2]. As their data only streches to a rate of 2 nm/s, it would be interesting to investigate if the observed trend holds for even higher rates.

The method proposed in this contribution is based on convective transport of radicals instead of diffusive, and has been used succesfully for fast deposition of diamond-like coatings [3]. Plasma production and deposition are geometrically separated, and in that sense it is related to the silicon deposition method described by Lucovsky et. al. using an inductively coupled plasma source [4,5] or the microwave cavity plasma source described by Johnson et. al. [6,7]: remote plasma enhanced chemical vapour deposition.

EXPERIMENTAL SETUP

The setup consists of a DC thermal arc plasma source and a low-pressure chamber (Fig. 1). A substrate holder, on which c-Si and Corning glass 7059 samples of approximately 2.5×2.5 cm^2 are attached, is mounted on a chuck in the deposition chamber through a load lock. Temperature is monitored using a thermocouple inserted in a dummy substrate mounted on the chuck.

Mat. Res. Soc. Symp. Proc. Vol. 377 © 1995 Materials Research Society

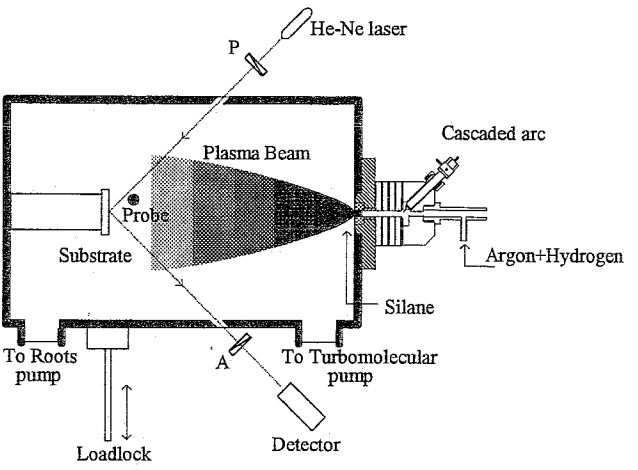

Fig. 1. Expanding plasma deposition setup

Plasma Source

The cascaded arc plasma source consists of three tungsten-thorium cathodes at one end, a stack of ten water cooled electrically insulated copper plates for thermal confinement of the plasma, and an anode plate at the other end. Through the copper plates and the anode plate there is a 4 mm bore, forming a cylindrical channel of 6 cm. The plasma is generated by a DC discharge (typically 50A, 100V) between the three cathodes and the anode. As the arc is operated at a typical pressure of 0.5 bar, the plasma is close to local thermal equilibrium and characterized by a high electron density and low electron temperature ($n_e \approx 10^{22}$ m^{-3}, $T_e \approx 1$ eV). It can flow into the deposition chamber through a parabolically shaped nozzle in the anode plate.

In the plasma source, an argon/hydrogen mixture is used as feed gas. Hydrogen will be dissociated and partially ionized both by electron collisions and by collisions with argon ions; as the ionization energy of argon (15.76 eV) is higher than that of hydrogen (13.6 eV) and collision rates are high, no argon ions are expected to remain when the hydrogen flow exceeds 5% of the total flow; therefore the presence of argon in the feed gas does not result in bombardment of the substrate surface.

The Expanding Plasma Jet

The plasma expands supersonically into the deposition chamber (pressure typically 20 Pa), shocks and flows subsonically towards the substrate with a typical transport velocity of 10^3 m/s [8]. At the position of the substrates (32 cm downstream from the nozzle), the plasma beam has a diameter of about 30 cm. In the argon/hydrogen plasma jet, typical downstream plasma parameters (determined with a Langmuir probe and confirmed by Thomson scattering) are an electron density of about 10^{17} m^{-3} and an electron temperature of about 0.2 eV. Pure silane is injected into the jet just behind the expansion nozzle.

Since due to the low electron temperature dissociation of silane by electron collisions is negligible, we believe that dissociation (or ionization) of silane is achieved by two possible routes: hydrogen abstraction:

$$SiH_4 + H \rightarrow SiH_3 + H_2 \qquad (\Delta E = -0.5eV) \tag{1}$$

or a sequence of dissociative charge exchange and consecutive dissociative recombination, e.g.:

$$\begin{aligned} SiH_4 + H^+ &\rightarrow SiH_3^+ + H_2 \qquad (\Delta E = -5.8eV) \\ SiH_3^+ + e^- &\rightarrow SiH_2 + H \qquad (\Delta E = -5.4eV) \end{aligned} \tag{2}$$

The reaction rate constant for reaction (2) is more than two orders of magnitude larger than the rate constant for reaction (1) [9]. Nevertheless, for our standard setting, the H/H^+ ratio is even larger [10], and therefore it is believed that before silane injection, the dominant chemically active species is the hydrogen atom. It must be noted that if the SiH_4/H ratio or the mean free path becomes small, the hydrogen abstraction reaction can lead to lighter radicals such as SiH_2 or SiH.

Another difference in comparison to other deposition plasmas is the low energy of ions impinging on the substrate, typically less than 2 eV, thus excluding significant ion bombardment. This is due to a low substrate self-bias as a result of the low electron temperature.

Diagnostics

The plasma is monitored using a Langmuir probe and a photon counting setup for emission spectroscopy. In a similar machine devoted to argon/hydrogen expanding plasma jets, more elaborate plasma measurements such as Thomson-Rayleigh scattering are performed [10].

Growth rate and refractive index of the deposited layer are monitored in-situ using a Rotating Analyzer ellipsometer at 632.8 nm. Ex-situ layer analysis include optical transmission measurements, determination of photo- and dark conductivity and Fourier Transform Infra Red transmission (FTIR) measurements. Analysis of the FTIR spectra is similar to the method described by Langford et. al. [11]; the same proportionality constants have been used. From the 640 cm^{-1} wagging mode the hydrogen concentration is determined, and the 2000 cm^{-1} and 2100 cm^{-1} stretching modes yield the SiH and SiH_2 concentrations respectively. The hydrogen concentration is also determined using Elastic Recoil Detection Analysis (ERDA), with 4 MeV alpha particles. ERDA with 13.4 MeV alpha particles gives the oxygen impurity concentration.

RESULTS

A first optimization scan through the operation parameter range (argon flow, hydrogen flow, silane flow and arc current) resulted in a setting of $Ar:H_2:SiH_4$ = 55:10:6 scc/s and an arc current of 45 A to yield the highest refractive index at 632.8 nm, as measured by in-situ ellipsometry. Film uniformity has, as yet, not been investigated. Chamber pressure and dummy substrate temperature are kept constant at 20 Pa and 250 °C respectively. The measurements presented here are performed on samples deposited at this setting, with the exception of a variation of the hydrogen flow around the optimum setting.

Table I gives an overview of achieved material properties. Stated are the growth rate, the refractive indices at 632.8 nm and in the infrared, the hydrogen concentration determined from the 640 cm^{-1} wagging mode, the ratio of the stretching modes (so-called microstructure parameter), the full width half maximum of the 2000 cm^{-1} peak, the optical bandgap according to Tauc's definition, the photoconductivity under AM1.5 illumination, the photoresponse, the dark conductivity activation energy, the oxygen content from ERDA (at this moment detection limit is 0.3%), the density of states at midgap as determined from a thermally stimulated conductivity measurement (no light soaking) and the electron mobility lifetime product.

Table I. Overview of achieved material properties

growth rate	15 nm/s	σ_{photo}	$10^{-6}\ \Omega^{-1}cm^{-1}$
n_{HeNe}	4.2	$\sigma_{photo}/\sigma_{dark}$	10^{6}
n_{IR}	3.3	E_{act}	0.8-1 eV
[H]	10%	[O]	<0.3%
$I_{2100}/(I_{2000}+I_{2100})$	0.2	DOS_{midgap}	$3\cdot10^{16}\ cm^{-3}$
FWHM(I_{2000})	110 cm^{-1}	$\mu\tau$ (300 K)	$10^{-6}\ cm^{2}V^{-1}$
$E_{gap,\ Tauc}$	1.7 eV		

Figure 2 depicts the refractive index (both at 632.8 nm and in the infrared) versus the hydrogen content from the 640 cm^{-1} mode, and figure 3 shows the corresponding SiH and SiH_2 concentrations. As the hydrogen content increases, material quality decreases. Transmission Electron Microscopy (TEM) measurements on two representative samples have shown that the

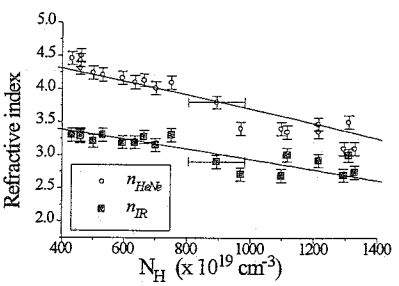

Fig. 2. Refractive index at 632.8 nm and in the infrared vs. hydrogen content. Solid lines are a guide to the eye.

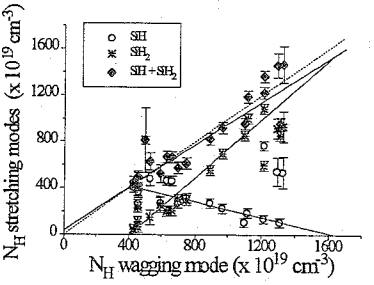

Fig. 3. The SiH and SiH_2 content vs. total hydrogen content. Solid lines are linear fits; the dashed line corresponds to x=y

structure of a layer with 8% hydrogen is amorphous and comparable to PECVD-grown device quality material, whereas a layer with 23% hydrogen exhibits a columnar structure.

Figures 4 and 5 show respectively the growth rate and the Langmuir probe ion saturation current as a function of hydrogen flow into the plasma. From the observed decrease of ion saturation current and simultaneous increase of deposition rate, we tentatively conclude that the contribution of ions as a primary growth precursor is small.

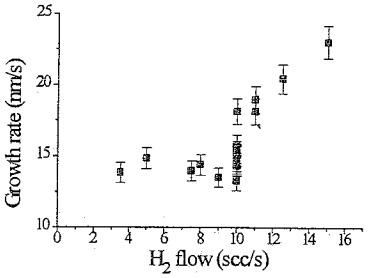

Fig. 4. Growth rate vs. hydrogen flow

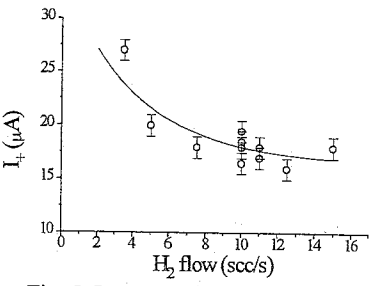

Fig. 5. Langmuir probe ion saturation current vs. hydrogen flow

It appears that an important role in the growth kinetics is played by hydrogen in the feed gas. To gain a better understanding of the incorporation of hydrogen in the growing film of feed gas hydrogen, a number of deposition runs have been done using D_2 instead of H_2. It was found that the material becomes significantly less dense: the refractive index drops considerably, at 632.8 nm to about 3 and in the infrared to 2.6. The growth rate increases considerably to 35 nm/s; such a rise in growth rate when using D_2 instead of H_2 in a remote hydrogen plasma is also reported by Ready et. al. [12]. Deuterium related infrared absorption peaks at 790 cm^{-1}(SiHD bending) and 1525 cm^{-1} (SiD_2 and SiHD stretching) are very small compared to the hydrogen related peaks. When using a proportionality constant $A_{Si\text{-}D}$ that is twice as large as the $A_{Si\text{-}H}$ proportionality constants for hydrogen [13], we find that the D/H-ratio is in the range of 0.1±0.05, a value that is confirmed by ERDA. It appears that deuterium incorporation is of minor importance, as was also observed by Johnson when using a D_2/SiH_4=1 feed gas ratio [6]. Turban et. al. [13] argue that there are in principle two mechanisms of deuterium incorporation: gas phase reactions such as the displacement reaction

$$D + SiH_3 \rightarrow SiH_2D + H \qquad (3)$$

and direct incorporation into the film either by breaking weak Si-Si bonds or by a D/H exchange reaction. The importance of the heterogeneous reaction is demonstrated by their mass spectrometry measurements on a PECVD setup: it was found that the D/H ratio in the gas phase deuterated silanes was less than 0.2 (feed gas ratio D_2/SiH_4 was 20), whereas this ratio in the a-Si:H:D layer was, according to FTIR analysis, about 0.6. Nevertheless it appears that the most important reaction of atomic H or D at the surface is abstraction.

It must be noted that when using D_2 instead of H_2, due to the mass difference the kinetics of the plasma source change. A cleaner experiment would be to keep the plasma source unaltered (i.e. using an argon/hydrogen mixture) and to inject SiD_4 into the plasma jet. It is expected that under optimum settings the hydrogen-related infrared absorption peaks become small.

DISCUSSION

From the listed material properties it is observed that, after a first optimization round, growth rate is an order of magnitude higher than more conventional techniques such as VHF-PECVD and comparable to microwave PECVD [14], but also that the material contains more defects than state-of-the-art device grade material. The presence of polyhydrides is known to be associated with a lower mobility-lifetime product [5], leading to a lower photoconductivity. However, a number of parameters such as substrate temperature and chamber pressure are still to be optimized, as is the gas feed geometry.

ACKNOWLEDGEMENT

This research was financially supported by the Netherlands Organization for Energy and the Environment (NOVEM). The work of M.C.M. van de Sanden is made possible by the Netherlands Academy for Arts and Sciences. The authors wish to thank K. Feenstra, J. Wallinga, D. Knoese, W.G.J.H.M. van Sark, E.A.G. Hamers, L.J. van IJzendoorn and A.J.H. Maas for their contributions, and M.J.F. van de Sande, A.B.M. Husken and H. de Jong for their skillful technical assistance.

REFERENCES

1. Y. Ichikawa, K. Tabuchi, S. Kato, A. Takano, T. Sasaki, M. Tanda, S. Saito, H. Sato, S. Fujikake, T. Yoshida and H. Sakai, Proc. 1st World Conference on Photovoltaic Energy Conversion, Waikoloa, Hawaii (1994)
2. G. Ganguly and A. Matsuda, Jpn. J. Appl. Phys. **31**, 1269 (1992); J. Non-Cryst. Solids **164-166**, 31 (1993)
3. G.M.W. Kroesen, D.C. Schram and M.J.F. van de Sande, Plasma Chem. and Plasma Proc. **10** (1) 49 (1990)
4. G. Lucovsky, P.D. Richard, D.V. Tsu, S.Y. Lin and R.J. Markunas, J. Vac. Sci. Technol. A4 **3** 681 (1986)
5. G.N. Parsons, D.V. Tsu and G. Lucovsky, J. Non-Cryst. Solids **97-98**, 1375 (1987)
6. N.M. Johnson, J. Walker, C.M. Doland, K. Winer and R.A. Street, Appl. Phys. Lett. **54** (19) 1872 (1989)
7. N.M. Johnson, P.V. Santos, C.E. Nebel, W.B. Jackson, R.A. Street, K.S. Stevens and J. Walker, J. Non-Cryst. Solids **137-138** 235 (1991)
8. M.C.M. van de Sanden, J.M. de Regt and D.C. Schram, Phys. Rev. E **47** 2792 (1993)
9. M.J. Kushner, J. Appl. Phys. **63** (8) 2532 (1988)
10. R.F.G. Meulenbroeks, A.J. van Beek, A.J.G. van Helvoort, M.C.M. van de Sanden and D.C. Schram, Phys. Rev. E **49** 4397 (1994)
11. A.A. Langford, M.L. Fleet, B.P. Nelson, W.A. Lanford and N. Maley, Phys. Rev. B **45** (23) 13367 (1992)
12. S.E. Ready, J.B. Joyce, N.M. Johnson, J. Walker and K.S. Stevens, Mat. Res. Soc. Symp. Proc. **192** (1990)
13. G. Turban, Y. Catherine and B. Grolleau, Thin Solid Films **77**, 287 (1981)
14. S. Guha, X. Xu, J. Yang and A. Banerjee, see elsewhere in these proceedings